Laughlin, L., Zhang, C. J., Beach, M., Morris, K., & Haine, J. (2017). Electrical Balance Duplexer Field Trials in High-Speed Rail Scenarios. *IEEE Transactions on Antennas and Propagation*, *65*(11), 6068-6075. https://doi.org/10.1109/TAP.2017.2748224

Electrical Balance Duplexer Field Trials in High Speed Rail Scenarios

Leo Laughlin, *Member, IEEE,* Chunqing Zhang, *Member, IEEE,* Mark A. Beach, *Member, IEEE,* Kevin A. Morris, *Member, IEEE,* and John L. Haine, *Member, IEEE*

***Abstract*—Electrical balance duplexers (EBDs) present a potential alternative to the fixed frequency duplexing filters used for frequency division duplexing in cellular handset radio frequency front-ends. However the transmit-to-receive (Tx-Rx) isolation can be affected by interaction between the antenna and the environment, and therefore the EBDs *balancing impedance* must adaptively track time domain antenna impedance variation. A rail scenario presents a potentially demanding use case for an EBD, as fast moving trains in the vicinity of the antenna may cause dynamically changing reflections which can be received as self-interference. In this paper, measured dynamic antenna reflection coefficients at 745 MHz and 1900 MHz from train mounted antennas are included in EBD circuit simulations in order the investigate the resulting variation in Tx-Rx isolation, and determine requirements for balancing impedance adaptation. This paper also presents results from rail based field trials of a hardware prototype EBD which implements real time antenna impedance tracking. Results show that the rail scenario does result in variation in Tx-Rx isolation, but that re-balancing the EBD at intervals of 5 ms was sufficient to maintain >50 dB isolation for ∼95% of the time.**

***Index Terms*—Duplexers, Electrical Balance Duplexer, Self-interference cancellation, 5G enabling technologies.**

I. Introduction

FREQUENCY DIVISION DUPLEX (FDD) Radio Frequency (RF) front-end designs employed in today's cellular handsets achieve duplex operation using discrete, fixed-frequency surface acoustic wave (SAW) or bulk acoustic wave (BAW) filters. State of the art tunable filters cannot meet the demanding requirements for steep roll-off and low insertion loss [1]; supporting multi-band operation therefore requires multiple separate fixed frequency duplexers and switches for band selection [2]. Third Generation Partnership Project (3GPP) Long Term Evolution (LTE) currently defines 30 FDD bands [3], however supporting all of these bands with the current architecture is both technically infeasible and commercially unviable, as the resulting circuit would be prohibitively large, lossy, and expensive. Consequently, smartphones currently only support a region specific subset of bands, increasing manufacturing costs, and preventing unrestricted global roaming on LTE [2]. Producing a tunable RF front-end is a key challenge for the next generation of mobile devices.

Electrical Balance Duplexers (EBDs) [4]–[18] implement a form of self-interference (SI) cancellation in order to provide high transmit-to-receive (Tx-Rx) isolation. Recent advances have exhibited on-chip EBDs with tunability, insertion loss, noise figure, receiver linearity, and blocker rejection characteristics suitable for mutliband cellular duplexing applications [4], [5], [18], demonstrating EBDs are a viable alternative to fixed frequency filters in FDD transceivers. The EBD is also applicable to in-band full-duplex transceiver designs [13], [19], where is can be used as the first stage of self-interference cancellation. The isolation provided by the EBD depends on very close matching of the antenna and *balancing impedance*. Due to interaction with the local environment, the antenna impedance is time variant, and consequently the balancing impedance must adaptively track the antenna impedance in order to maintain isolation [8], [10]–[13], [20] (see Fig. 1). Thus, in order to specify an effective balancing impedance tracking sub-system, it is necessary to investigate dynamic antenna impedance variation, and its effect on Tx-Rx isolation, over the range of intended operating environments.

Previous contributions on this topic have combined EBD circuit simulations with antenna reflection coefficient measurements from dynamic environments to investigate adaptation requirements in handheld [10], indoor [11], and road vehicle scenarios [12]. Results demonstrated that antenna impedance tracking was critical in the user interaction scenario, requiring the EBD to be rebalanced at intervals of the order of 10 ms to maintain isolation, but adaptation was not essential in the indoor and road environments, due to the larger separation between the antenna and the reflecting objects [11], [12].

This paper presents an analysis of Tx-Rx isolation performance in a high speed rail scenario. Due to close proximity of passing trains and trackside infrastructure, a rail scenario has the potential to cause more substantial variation in the antenna impedance compared to the road scenario, and warrants investigation into the variation in Tx-Rx isolation and balancing impedance adaptation requirements in this scenario. The analysis methodology from [10]–[12], in which measured antenna dynamics are embedded into EBD circuit simulations, has been repeated for a high speed rail scenario. Furthermore, this paper also presents a hardware EBD with real time balancing impedance tracking, and demonstrates measured dynamic EBD performance in the high speed rail application. This is the first hardware EBD with real time impedance tracking to be tested in a realistic dynamic environment.

Manuscript received October 30, 2016; Revised June 20 2017, Accepted August 11 2017. This research is supported in part by the UK Engineering and Physical Sciences Research Council (EP/K503824/1), and in part by u-blox AG.

The authors are with the Department of Electrical and Electronic Engineering, University of Bristol, BS8 1UB, UK. e-mail: Leo.Laughlin@bristol.ac.uk.

Color versions of one or more of the figures in this paper are available online at http://ieeexplore.ieee.org.

Measurement data published: 10.5523/bris.wna9731drfr72agb5nu3zx2fy

Digital Object Identifier:

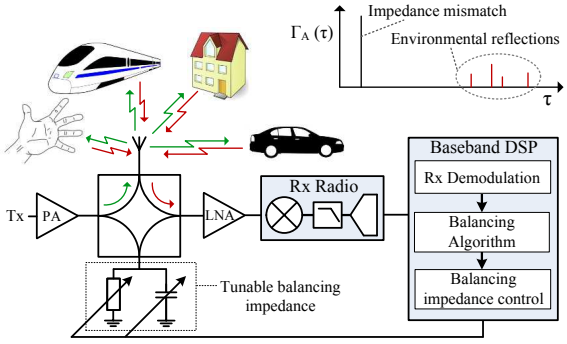

Fig. 1. An EBD with adaptive balancing impedance control in a dynamic reflective environment. Inset graph illustrates the antenna reflection coefficient impulse response, $\Gamma_A(\tau)$, showing the main reflection due to mismatch with the antenna itself, and reflections from objects in the surrounding environment.

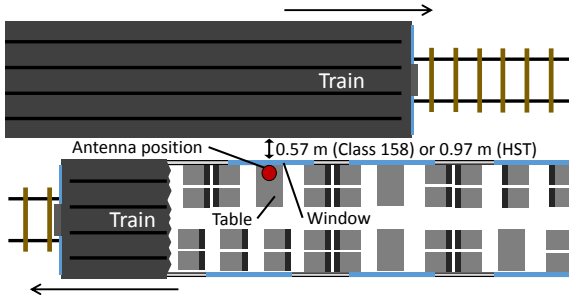

Fig. 2. Antenna position on board the train used in this investigation. This antenna position is used to investigate the worst case scenario for dynamic environmental reflection in the rail application, in which the device is being used close to a window (e.g. with the user sitting in the window seat) as another train passes in the opposite direction on an adjacent track.

The remainder of this paper is organised as follows. Section II details antenna measurements and circuit simulations from the high speed rail scenario, and Section III presents and analyzes the simulation results, showing that even in the highly dynamic rail environment adaptive EBDs are effective at maintaining isolation. Section IV describes the hardware EBD with high speed antenna impedance tracking. Section V presents hardware results, validating the simulations. Section VI concludes.

II. Simulated Tx-Rx Isolation with Measured Antenna Dynamics

To investigate performance variation due to the dynamic antenna reflection coefficient, antenna reflection coefficient measurements were taken on board high speed trains for use in EBD circuit simulations. Of particular interest is the scenario where the antenna is close to the window (e.g. a mobile device user in a window seat) with another train passing on the adjacent track; this could be within 1 m of the antenna and therefore may have a substantial impact on EBD isolation (see Fig. 2). The antennas selected for use in this investigation were two dipole antennas, one designed for operation at 745 MHz and the other for operation at 1900 MHz. The use of two dipole antennas at two different frequencies allows differences between the results from different frequencies to be attributed to the differences in propagation behaviour only. This is not possible with a multiband antenna, as this type of antenna will exhibit different patterns and efficiencies at different frequencies. Measurements were conducted on two types of train: the British Rail High Speed Train (HST) - also know as the "Intercity 125" - and the British Rail Class 158. Neither of these trains have metallized tinted windows. The Class 158 train measurements were conducted on the Wessex Main Line between Bristol and Southampton, which has a maximum speed of 90 mph (145 km h^{-1}). The HST measurements were conducted on the Great Western Main Line between Bristol and London, which has a maximum speed of 125 mph (201 km h^{-1}). The antenna was raised to the height of the window using a plastic box placed atop the cabin table, as shown in Fig. 3. The antenna was mounted 10 cm from the window glass.

Antenna reflection coefficient measurements were performed using a National Instruments vector signal transceiver configured to operate as a vector network analyzer (VNA), measuring the antenna reflection coefficient at 745 MHz or 1900 MHz, with a measurement bandwidth of 20 MHz and frequency resolution of 100 kHz. Since the dominant limitation in EBD isolation is the imperfect matching between the antenna and balancing impedances [7], RF imperfections and noise in these measurements have no substantial impact on the isolation results. In order to capture the time domain variation due to environmental interaction, the antenna S_{11} frequency response measurement was repeated at sampling intervals of 0.5 ms (i.e. a 2 kHz sampling rate)[1]. Measurements were taken with and without a train passing in the opposite direction on the adjacent track. The gap between passing trains is 57 cm for the Class 158 and 97 cm for the HST (see Fig. 2).

A. Simulated EBD

The resulting antenna measurement data comprises a time series of antenna S_{11} frequency responses. This data is then incorporated in to an EBD circuit simulation to provide a highly realistic model of the variable antenna reflection coefficient. The simulation assumes a symmetrical, lossless hybrid junction, and ideal continuously variable lumped element components in the tunable balancing impedance circuit, and calculates the mean Tx-Rx isolation across a 20 MHz band as a function of time[2]. This EBD circuit simulation is identical to the simulations presented previously in [10]–[12], allowing for direct comparison of results. A more comprehensive description of the EBD simulation can also be found in these references. As was the case in [10]–[12], the simulation implements three balancing impedance adaptation characteristics: *ideal balancing*, where the balancing

[1]It can be shown that this is more than sufficient to prevent aliasing at the speeds and frequencies involved in this measurement campaign.

[2]This simulation, and also the hardware EBD described in section IV, operate over a single contiguous band, rather than in two separate bands as required by an FDD application. However, since EBDs in the FDD application require simultaneous *independent* control of the balancing impedance in both the uplink and downlink bands (e.g., [6], [17], [18]), the analysis presented here is also directly relevant to the FDD application, being representative of performance in either one of the uplink or downlink bands.

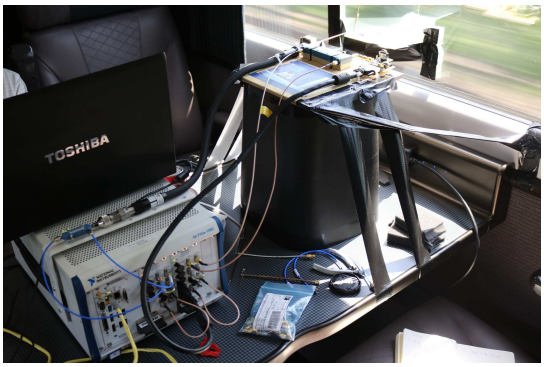

Fig. 3. Photograph of the measurement setup positioned on top of a cabin table inside a train.

impedance always takes on the optimal value, *static balancing*, where the balancing impedance is not dynamically adjusted to track antenna impedance changes, and *limited rate adaptation (LRA)*, where the balancing impedance is updated at a given interval, thus allowing the trade-off between EBD re-balancing rate and Tx-Rx isolation to be observed. The duration of the simulations is approximately 2 s, this being determined by the time taken for a train to pass.

III. Simulation Results

Fig. 4 plots the cumulative distribution functions of the Tx-Rx isolation, showing the variation of the Tx-Rx isolation over the the duration of the simulations. In all simulations (Figs. 4a, 4b, 4c and 4d), it can be noted that, when no train is passing, the statically balanced EBD achieves substantially the same performance as the EBD with ideal antenna impedance tracking, thereby demonstrating that *when no train is passing, balancing impedance adaptation is not required* (for this reason results for LRA are not plotted for the cases without a train passing). Comparing the 745 MHz simulations for the two different train types (Figs. 4a and 4c), it can be seen that, when no train is passing, slightly more variation was observed on the HST (Fig. 4a), with isolation varying between 44 dB and 46 dB, whereas for the Class 158 train, the isolation barely varied at all, remaining at approximately 45 dB throughout. This can be attributed to the difference in track-side infrastructure between the two lines: the Great Western Main Line on which the HST measurements were conducted is electrified, and therefore has many stanchions to support the overhead cables, whereas the Wessex Main Line is not electrified and therefore has far fewer track-side structures, and thus fewer dynamic reflections returning energy to the antenna, leading to less variation.

A. Reflections from train interior

Observing Fig. 4d, it is notable that the 1900 MHz simulations for the Class 158 trains achieved significantly higher isolation compared to the same analysis from the HSTs. Such large differences can only be attributed to differences in the local environment (i.e. within the train). Although care was taken to mount the antennas in the same configuration in both train types, the different shape, construction, and materials used in the two different types of train will inevitable lead to differing reflections from the interior of the train. For example, the windows are different sizes in the two trains, and thus reflections from the nearby metal window frames will be different between the two types of train. Reflections in indoor environments can substantially affect the isolation (see [7], [8]), leading to this difference between the two trains types at 1900 MHz.

B. Passing trains

On the HST at 745 MHz (Fig. 4a), the passing train did result in substantially more variation in Tx-Rx isolation compared to the case with no train passing, varying from 40-50 dB, however, the impact is not catastrophic, and even in the statically balanced case, the isolation remains above 40 dB. In the ideal balanced case, the isolation still varies substantially, as even with optimal settings the single pole balancing network does not have the capability to cancel all of the reflected energy, and thus the SI channel varies according to instantaneous antenna reflection coefficient response and is only, on average, approximately 2 dB better than the statically balanced case. The 100 ms rebalancing interval resulted in Tx-Rx isolation being, on average, within 1 dB of the ideal case. From these results it is possible to conclude that *achieving >40 dB of isolation does not require balancing impedance adaptation in this scenario* and that *achieving near optimal performance does not require a very fast (i.e. kHz) balancing impedance adaptation rate*. The same analysis at 1900 MHz (Fig. 4b showed the train has a much smaller impact, reducing isolation by 1-2 dB compared to the case without a passing train. Furthermore, even with the passing train, the static balancing achieved substantially the same performance as the EBD with ideal balancing adaptation, demonstrating that at 1900 MHz, balancing adaptation is also not required at this level of isolation in this environment.

The same analysis for the Class 158 train at 745 MHz (Fig. 4c), shows that the passing train has more impact on the isolation. The statically balanced EBD saw a greater reduction in isolation compared the HST analysis, and in this case there is a larger difference between the static EBD and adaptive EBDs: the ideal EBD provides on average 5 dB of additional isolation. However, again, achieving >40 dB of isolation in this environment did not require very high speed balancing impedance adaptation, with a 100 ms re-balancing interval providing isolation within 2 dB of the ideal case, and a 5 ms re-balancing interval providing isolation within 1 dB of the ideal case. The larger impact of the passing train observed on the Class 158 train as compared to the HST can be attributed the gap between passing Class 158 trains being smaller, thereby resulting in higher reflected power.

Fig. 4d demonstrates larger variation in isolation compared the the same analysis from the HST (Fig. 4b), with the statically balanced EBD being, on average, 5-7 dB worse than the ideal EBD when a train is passing. This can again be attributed to the higher powered reflections on the class 158 due to the smaller gap between passing trains. The 5 ms re-balancing interval is again sufficient to obtain isolation within

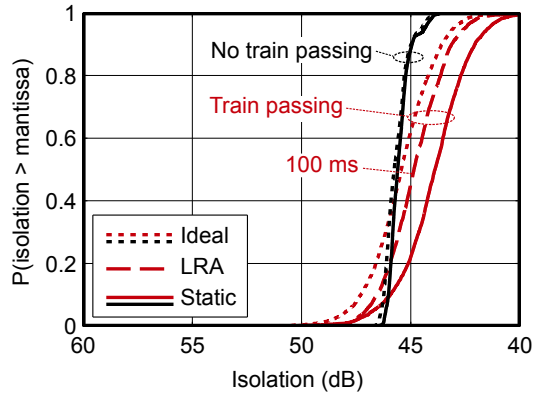

(a) HST, 745 MHz, simulated EBD.

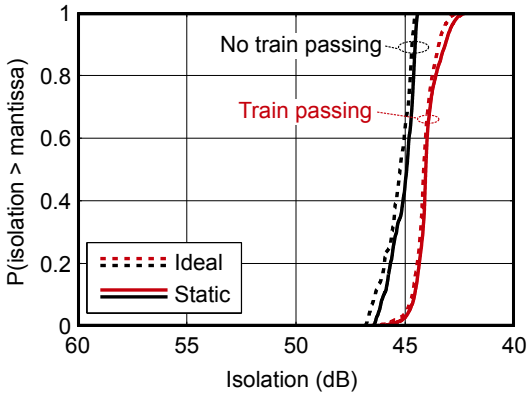

(b) HST, 1900 MHz, simulated EBD.

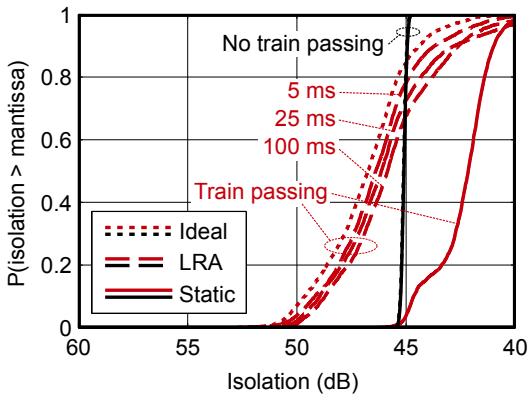

(c) Class 158, 745 MHz, simulated EBD.

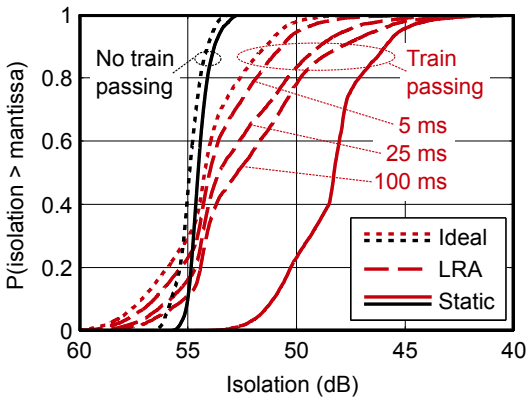

(d) Class 158, 1900 MHz, simulated EBD.

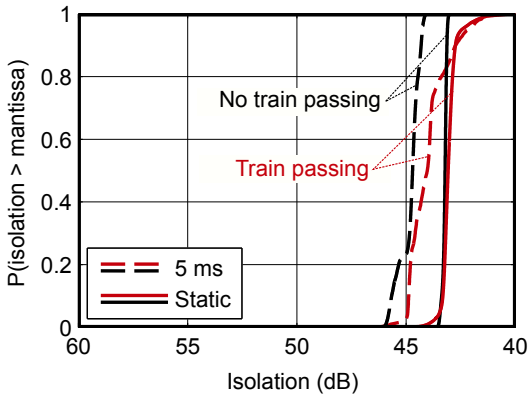

(e) Class 158, 745 MHz, hardware EBD.

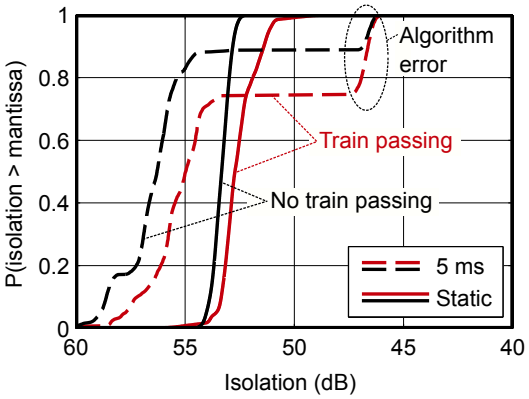

(f) Class 158, 1900 MHz, hardware EBD.

Fig. 4. Cumulative distribution functions of simulated and measured Tx-Rx isolation. (a): Simulated results from the high speed train at 745 MHz, with and without another train passing in the opposite direction on the adjacent track, when using ideal balancing, static balancing or limited rate adaptation with a re-balancing interval of 100 ms. Results for rebalancing intervals of 5 ms and 25 ms showed very similar performance to 100 ms, and are therefore not shown. (b): Simulated Tx-Rx isolation for an adaptive EBD on board the high speed train at 1900 MHz, with and without another train passing in the opposite direction on the adjacent track, when using ideal balancing and static balancing. Since the ideal and static balancing results are very similar, limited rate adaptation is not plotted. (c): Simulated Tx-Rx isolation for an adaptive EBD on board the Class 198 train at 745 MHz, with and without another train passing in the opposite direction on the adjacent track, when using ideal balancing, static balancing, or limited rate adaptation with re-balancing intervals of 5 ms, 25 ms, and 100 ms. (d): Same as (c) but at 1900 MHz. (e): Measured Tx-Rx isolation of the hardware EBD on the Class 198 train at 745 MHz, with and without another train passing in the opposite direction on the adjacent track, and when using static balancing or adaptive balancing with 5 ms rebalancing intervals. (f): Same as (e) but at 1900 MHz.

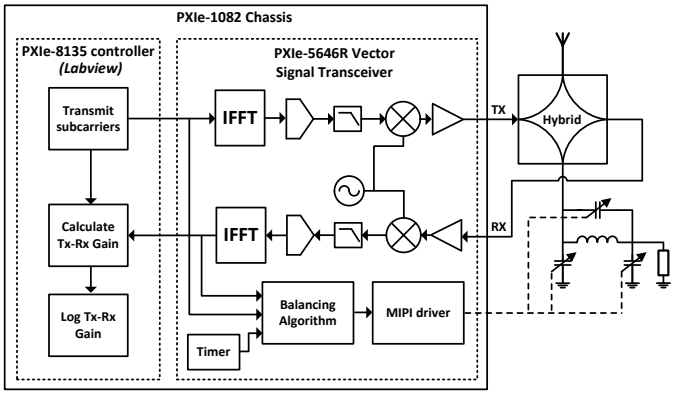

Fig. 5. Block diagram of the vector signal transceiver based hardware EBD with high speed balancing impedance adaptation.

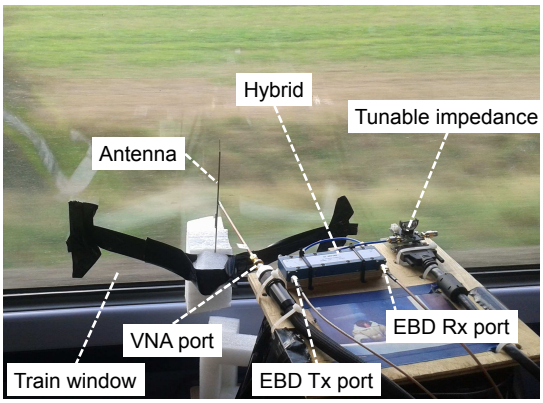

Fig. 7. Photograph of the hardware EBD mounted in the window of a train.

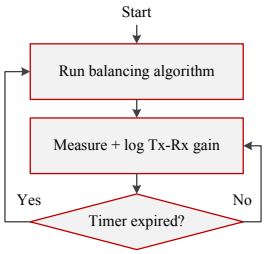

Fig. 6. Flowchart of adaptive EBD operation. The system runs the balancing algorithm at periodic intervals and then measures and logs the Tx-Rx isolation in the intervening time.

1 dB of the ideal balancing adaptation. It is also pertinent to note that the higher isolation observed in the 1900 MHz Class 158 analysis means that the EBD is more sensitive to variation in the antenna reflection coefficient, as, in comparison to an EBD with lower isolation, the same *magnitude* variation in the antenna reflection coefficient will result in a larger *relative reduction* (i.e. dB reduction) in isolation. This factor must be considered when comparing Fig. 4b against the same analysis for the 745 MHz case (Fig. 4a): although the dB variation is similar, with the range of variation in Tx-Rx isolation provided by ideal adaptation being approximately 10 dB in both, the absolute magnitude of this variation is much higher at the lower frequency, varying across 40-50 dB, as compared the the higher frequency, which saw isolation varying across 50-60 dB. Section VI.B below investigates the dynamic performance variation of a 745 MHz EBD which achieves 50-60 dB Tx-Rx isolation.

IV. Hardware EBD with High Speed Balancing Adaptation

In addition to the antenna measurement and simulation based analysis presented above, the Tx-Rx isolation achieved by a hardware implementation of an adaptive electrical balance duplexer was also measured in the high speed rail scenario. A block diagram of the hardware EBD is depicted in Fig. 5; the prototype is constructed from discrete components and is based around a National Instruments PXIe-5646R VST platform (programmed using LabView). The hybrid junction used is a Krytar model 1831 hybrid coupler, and the balancing circuit is a π-topology impedance tuning network constructed from 3 micro-electromechanical system (MEMS) digitally tunable capacitors and a fixed inductor, arranged as shown in Fig. 5, and terminated with a 50 Ω resistor. The inductor used is a 2.5 nH high-Q air-core surface mount component, and each of the 3 capacitors can be tuned from 0.46 pf to 5.69 pf in 0.1 pf steps. This tunable impedance offers extremely high resolution and wide Smith chart coverage; full details of the balancing network design and performance have been published in [21]. The transmitter and receiver sub-systems are implemented using the VST platform, utilising an orthogonal frequency division multiplexing (OFDM) physical layer to facilitate measurement of the Tx-Rx frequency response. The field programmable gate array (FPGA) within the VST is used to implement the required inverse fast fourier transform (IFFT) and fast fourier transform (FFT) operations required by OFDM. The FPGA is also used to implement the balancing algorithm presented in [16] in order to obtain the optimal balancing impedance settings, and a hardware driver to program the registers in the MEMS integrated circuit (IC), which is connected to the VST through the VST digital input/output port. The system runs the balancing algorithm at periodic intervals determined by a programmable timer, and in the intervening time, measures and logs the Tx-Rx isolation using the PXIe-8135 host controller with a sampling rate of 0.5 ms, allowing the variation in Tx-Rx isolation to be observed (see Fig. 6). The prototype also implements the static balancing behaviour, running the algorithm once at the beginning of a measurement, and then logging the measured Tx-Rx isolation without re-running the balancing algorithm.

The EBD hardware components were attached to a wooden mount, allowing the circuit to be easily secured to the tabletop platform. The VNA cable was also attached to the same wooden mount, such that the VNA port was immediately adjacent to the antenna port of the EBD. This can be seen in Fig. 7, which shows the EBD hardware and VNA cable mounted together in a train window. This allowed the antenna to be switched between the VNA and EBD port with minimal movement in the antenna position or the position of the objects next to antenna (i.e. the EBD hardware), thus ensuring the comparison between simulation and hardware measurements

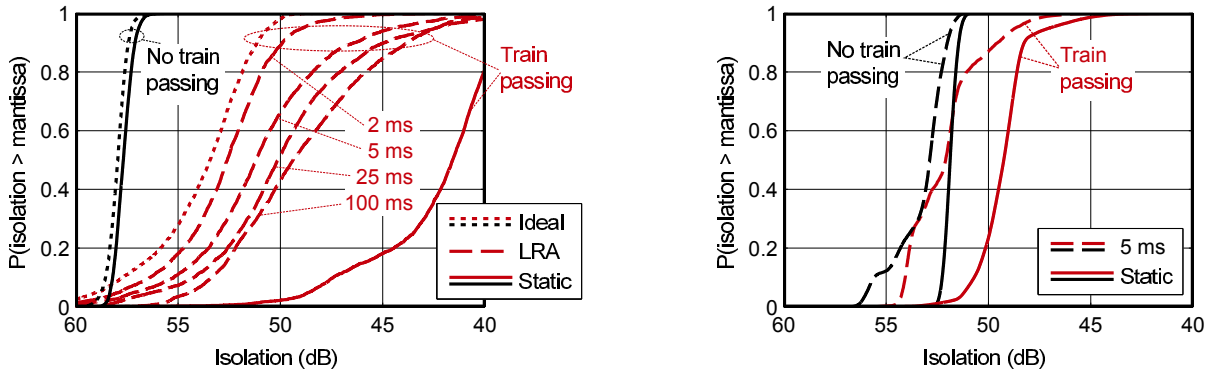

(a) Class 158, 745 MHz, simulated EBD, 5 MHz BW.

(b) Class 158, 745 MHz, hardware EBD, 5 MHz BW.

Fig. 8. Cumulative distribution functions of simulated and measured mean Tx-Rx isolation across a 5-MHz bandwidth at 745 MHz on board the Class 158.

is not compromised by disturbance of the local environment between the two measurements.

Measurements were taken using static balancing, and 5 ms rebalancing intervals, with and without another train passing in the opposite direction on the adjacent track, at 745 MHz and 1900 MHz. The duration of the measurements was approximately 2 s, this being determined by the time taken for a train to pass.

V. Hardware Results

CDFs of the measured Tx-Rx isolation from the adaptive hardware EBD on board the Class 158 train are plotted in Figs. 4e and 4f. In general the results are in agreement with the simulations presented above, validating the results given in Section IV, however there are some notable differences. For the 1900 MHz measurement (Fig. 4f), the statically balanced EBD shows similar performance in the case where there is no train, with both the simulation and hardware achieving 53-55 dB isolation. With a 5 ms re-balancing interval, the hardware EBD achieves, on average, better performance compared to the simulation, both with and without a passing train, however the isolation was observed to drop substantially in some measurements, as discussed in the following subsection. The isolation achieved by the statically balanced EBD when a train is passing is also slightly better than predicted by the simulation, and it is notable that in the statically balanced case, the isolation remained above 49 dB at all times, whereas the simulated isolation was observed to go as low as 42 dB. *This demonstrates that balancing impedance adaptation is not required to achieve $>\sim$50 dB isolation at 1900 MHz in a rail scenario*. As was the case with the simulation, the 745 MHz EBD (Fig. 4e) achieved lower isolation than the 1900 MHz EBD, with measured isolation ranging from 40-46 dB across all measurements. Again, the statically balanced hardware EBD performed slightly better in the case with the train passing compared to the corresponding simulated performance. The adaptive EBD provided, on average, lower isolation, however the minimum isolation observed over the measurement duration was higher than that of the simulation.

A. Balancing algorithm error

It is pertinent to note that, for the measured performance at 1900 MHz, there is a visible step-change in the Tx-Rx isolation CDFs, where the CDFs drop from approximately 54 dB isolation to approximately 47 dB, as circled on Fig. 4f. This may be attributable to error in the result of the balancing algorithm implemented by this hardware EBD. The algorithm used in this device (the linear version of the algorithm proposed in [16]) uses two sequential measurements of the SI channel to directly calculate the value of the balancing impedance required to maximize isolation. However, this algorithm relies on the assumption that the antenna reflection coefficient does not vary significantly between these two measurements (which are taken 1 ms apart in this implementation). It is possible that the variation in antenna reflection coefficient due to environmental interaction leads to a close, but non-optimal solution in a small number of cases. The error occurs in 23% of cases when a train is passing, and 5% of cases when there is no train, supporting the hypothesis that this is caused by the environmental disturbance. This error could be mitigated by averaging the result of multiple runs of the algorithm.

Balancing algorithm error was not observed in the 745 MHz measurements: this may be due to the larger wavelength results in slightly slower variations in the antenna reflection coefficient, allowing the quasi-stationary assumption to hold at this frequency.

B. Analysis for 5-MHz bandwidth

Neither the simulated or measured Tx-Rx isolation for the 745 MHz system achieved $>$50 dB isolation across a 20 MHz bandwidth, due to the poor isolation bandwidth achieved when using the 745 MHz antenna. As mentioned in IV.B, the sensitivity to environmental interaction depends on the absolute value of the isolation, and thus for the 745 MHz analysis presented above it is not directly possible to ascertain adaptation requirements for a 745 MHz EBD with higher isolation than was achieved. However, this analysis can be performed by reducing the bandwidth of interest, which will provide higher average isolation across the band. This therefore allows the effect of the environment on EBDs with

higher isolation to be observed, and the conclusions which can be drawn from this are also relevant to EBDs which achieve similar levels of isolation over wider bandwidths by employing a more complicated balancing network design with a larger number of tunable elements [9], [13].

Figs. 8 plots simulated and measured Tx-Rx isolation over a 5 MHz bandwidth centred at 745 MHz (i.e. a frequency domain subset of the results presented above). These plots exhibit higher isolation, allowing comparison with the 1900 MHz results. The simulation result (Fig. 8a) clearly shows that the environment has a greater impact on the Tx-Rx isolation at 745 MHz compared to 1900 MHz (i.e. Fig. 4d), which can be attributed to the reduced propagation loss of environmental reflections at the lower frequency. The hardware EBD exhibits comparable performance, providing less isolation when no train is passing, but better isolation in the case where there is a train passing. The hardware result shows that a 5 ms rebalancing interval is adequate to provide $>$50 dB isolation for $\sim$95% of the time, which is slightly better than the simulation, which predicted this to be $<$70%. This demonstrates that *balancing impedance adaptation is necessary to maintain $>$50 dB isolation in the rail scenario at 745 MHz, but a 5 ms adaptation interval is adequate to maintain reasonable performance.*

VI. Conclusion

The transmit-to-receive isolation provided by an EBD is variable due to electromagnetic interaction between the antenna and the environment, and it is therefore necessary to characterise EBD performance in the intended operating environments. This paper has investigated performance in a high speed rail scenario, which is a potentially demanding use case due to the proximity of passing trains and trackside infrastructure.

Dynamically measured antenna reflection coefficient frequency responses of antennas mounted on moving trains have been embedded into EBD circuit simulations to determine EBD Tx-Rx isolation performance in this environment. Measured results from a hardware EBD with real time antenna impedance tracking on board a train have also been presented, validating the simulation results. The results demonstrate that passing trains can have a measurable impact on the EBD, causing variation in Tx-Rx isolation, however isolation performance can be maintained through balancing impedance adaptation, and the required adaptation rates are of the order of hundreds of Hz. At 1900 MHz, no balancing impedance adaptation was required to maintain $>\sim$50 dB of isolation when a train is passing close to the antenna, however at 745 MHz, a 5 ms rebalancing interval was required to maintain $>$50 dB isolation for $\sim$95% of the time.

Acknowledgment

The authors thank Taoglas for providing the cellular antenna, and Mr. K. Stevens for making the dipole antennas. The authors also express their profound gratitude to Great Western Rail for permission to perform experiments on-board their trains, and Mathew Gard for his support in doing so.

References

[1] R. Aigner, "Tunable Filters? Reality Check! Foreseeable Trends in System Architecture for Tunable RF Filters," *IEEE Microw. Mag.*, vol. 16, no. 7, pp. 82–88, Aug. 2015.

[2] J. Tsutsumi, M. Seth, A. S. Morris III, R. B. Staszewski, and G. Hueber, "Cost-Efficient, High-Volume Transmission: Advanced Transmission Design and Architecture of Next Generation RF Modems and Front-Ends," *IEEE Microw. Mag.*, vol. 16, no. 7, pp. 26–45, Aug. 2015.

[3] 3GPP, "Evolved Universal Terrestrial Radio Access (E-UTRA); User Equipment (UE) radio transmission and reception," 3rd Generation Partnership Project (3GPP), TS 36.101 v13.2.0, 01 2016.

[4] S. H. Abdelhalem, P. S. Gudem, and L. E. Larson, "Hybrid Transformer-Based Tunable Differential Duplexer in a 90-nm CMOS Process," *Microw. Theory Tech. IEEE Trans.*, vol. 61, no. 3, pp. 1316–1326, 2013.

[5] M. Mikhemar, H. Darabi, and A. A. Abidi, "A Multiband RF Antenna Duplexer on CMOS: Design and Performance," *Solid-State Circuits, IEEE J.*, vol. 48, no. 9, pp. 2067–2077, 2013.

[6] S. H. Abdelhalem, P. S. Gudem, and L. E. Larson, "Tunable CMOS Integrated Duplexer With Antenna Impedance Tracking and High Isolation in the Transmit and Receive Bands," *IEEE Trans. Microw. Theory Tech.*, vol. 62, no. 9, pp. 2092–2104, Sept. 2014.

[7] L. Laughlin, M. A. Beach, K. A. Morris, and J. L. Haine, "Optimum Single Antenna Full Duplex Using Hybrid Junctions," *IEEE J. Sel. Areas Commun.*, vol. 32, no. 9, pp. 1653–1661, Sept. 2014.

[8] L. Laughlin, M. Beach, K. Morris, and J. Haine, "Performance Variation in Electrical Balance Duplexers due to User Interaction," in *2014 IEEE 25th Annu. Int. Symp. Pers. Indoor, Mob. Radio Commun.*, Washington D.C, 2014, pp. 318–322.

[9] B. van Liempd, J. Craninckx, R. Singh, P. Reynaert, S. Malotaux, and J. R. Long, "A Dual-Notch +27dBm Tx-Power Electrical-Balance Duplexer," in *ESSCIRC 2014 - 40th Eur. Solid State Circuits Conf.* IEEE, Sept. 2014, pp. 463–466.

[10] L. Laughlin, M. A. Beach, K. A. Morris, and J. L. Haine, "Electrical balance duplexing for small form factor realization of in-band full duplex," *IEEE Commun. Mag.*, vol. 53, no. 5, pp. 102–110, May 2015.

[11] ——, "Electrical Balance Duplexer Adaptation in Indoor Mobile Scenarios," in *Proc. Eur. Conf. Antennas Propag.*, 2015.

[12] L. Laughlin, C. Zhang, M. A. Beach, K. A. Morris, and J. L. Haine, "Dynamic Performance of Electrical Balance Duplexing in a Vehicular Scenario," *IEEE Antennas Wirel. Propag. Lett.*, 2016.

[13] E. Manuzzato, J. Tamminen, M. Turunen, D. Korpi, F. Granelli, and M. Valkama, "Digitally-Controlled Electrical Balance Duplexer for Transmitter-Receiver Isolation in Full-Duplex Radio," 2016. [Online]. Available: http://ieeexplore.ieee.org/document/7499291/

[14] B. van Liempd, B. Hershberg, K. Raczkowski, S. Ariumi, U. Karthaus, K.-F. Bink, and J. Craninckx, "2.2 A +70dBm IIP3 single-ended electrical-balance duplexer in 0.18um SOI CMOS," in *2015 IEEE Int. Solid-State Circuits Conf. - Dig. Tech. Pap.* IEEE, Feb. 2015, pp. 1–3.

[15] T. Vermeulen, B. van Liempd, B. Hershberg, and S. Pollin, "Real-time RF self-interference cancellation for in-band full duplex," in *2015 IEEE Int. Symp. Dyn. Spectr. Access Networks*. IEEE, Sept. 2015, pp. 275–276.

[16] L. Laughlin, C. Zhang, M. A. Beach, K. A. Morris, and J. L. Haine, "Passive and Active Electrical Balance Duplexers," *IEEE Trans. Circuits Syst. II Express Briefs*, vol. 63, no. 1, pp. 94–98, Jan. 2016.

[17] B. Hershberg, B. van Liempd, X. Zhang, P. Wambacq, and J. Craninckx, "20.8 A dual-frequency 0.7-to-1GHz balance network for electrical balance duplexers," in *2016 IEEE Int. Solid-State Circuits Conf.* IEEE, Jan. 2016, pp. 356–357.

[18] B. van Liempd, B. Hershberg, S. Ariumi, K. Raczkowski, K.-F. Bink, U. Karthaus, E. Martens, P. Wambacq, and J. Craninckx, "A +70-dBm IIP3 Electrical-Balance Duplexer for Highly Integrated Tunable Front-Ends," *IEEE Trans. Microw. Theory Tech.*, pp. 1–13, 2016.

[19] A. Sabharwal, P. Schniter, D. Guo, D. W. Bliss, S. Rangarajan, and R. Wichman, "In-Band Full-Duplex Wireless: Challenges and Opportunities," *IEEE J. Sel. Areas Commun.*, vol. 32, no. 9, pp. 1637–1652, Sept. 2014.

[20] M. Mikhael, B. van Liempd, J. Craninckx, R. Guindi, and B. Debaillie, "A Full-Duplex Transceiver Prototype with In-System Automated Tuning of the RF Self-Interference Cancellation," in *Proc. 1st Int. Conf. 5G Ubiquitous Connect.* ICST, 2014, pp. 110–115.

[21] C. Zhang, L. Laughlin, M. Beach, K. Morris, and J. Haine, "Micro-Electromechanical Impedance Control for Electrical Balance Duplexing," in *Eur. Wirel. Conf.*, 2016.

Leo Laughlin received the M.Eng. degree in Electronic Engineering from the University of York, York, U.K., in 2011, and the Ph.D degree in Communications Engineering from the University of Bristol, Bristol, U.K., in 2016. In 2009-10 he was at Qualcomm in Farnborough, U.K., working on Physical Layer DSP for GSM receivers. In 2011 he was at Omnisense Ltd in Cambridge, working on radio geolocation systems. He is currently a Research Fellow in the Communications Systems and Networks Laboratory at the University of Bristol. His research interests are in tunable and reconfigurable radio technologies for mobile devices.

Chunqing Zhang was awarded the M.Sc. degree in Telecommunication and Information Systems from Beijing Jiaotong University, Beijing, China, in 2004. Between 2004 and 2014 he worked in the R&D department and the Testing department of Datang-Mobile Telecommunication Equipment Co. LTD., Beijing, China. Since 2014 he has been a Ph.D student and Research Assistant in the Communication Systems and Networks Laboratory, University of Bristol, Bristol, U.K.

Mark A. Beach Mark Beach received his PhD for research addressing the application of Smart Antenna techniques to GPS from the University of Bristol in 1989, where he subsequently joined as a member of academic staff. He was promoted to Senior Lecturer in 1996, Reader in 1998 and Professor in 2003. He was Head of the Department of Electrical and Electronic Engineering from 2006 to 2010, and then spearheaded Bristols hosting of the EPSRC Centre for Doctoral Training (CDT) in Communications. He currently manages the delivery of the CDT in Communications, leads research in the field of enabling technologies for the delivery of 5G and beyond wireless connectivity, as well as his role as the School Research Impact Director. Marks current research activities are delivered through the Communication Systems and Networks Group, forming a key component within Bristols Smart Internet Lab. He has over 25 years of physical layer wireless research embracing the application of Spread Spectrum technology for cellular systems, adaptive or smart antenna for capacity and range extension in wireless networks, MIMO aided connectivity for through-put enhancement, Millimetre Wave technologies as well as flexible RF technologies for SDR modems underpins his current research portfolio.

Kevin A. Morris received the B.Eng. and Ph.D. degrees in electronics and communications engineering from the University of Bristol, Bristol, U.K., in 1995 and 2000, respectively. He is currently a Reader of RF engineering and Head of the Department of Electrical and Electronic Engineering, University of Bristol. He has authored or co-authored 90 academic papers and he holds five patents. His research interests principally concern looking at methods of reducing power consumption in communications systems including the area of RF hardware design with a specific interest in the design of efficient linear broadband power amplifiers for use within future communications systems. Dr. Morris is currently involved with a number of the Engineering and Physical Sciences Research Council (EPSRC) research programmes including FARAD and SENSE and industry funded research programmes within the U.K. He is a member of the UK Electronic Skills Foundation (UK-ESF) Strategic Advisory board.

John L. Haine is Royal Academy of Engineering Professor in Electrical and Electronic Engineering at the University of Bristol. He graduated with B.Sc (1971) and Ph.D (1977) degrees from Birmingham and Leeds Universities in the UK. He has worked on wireless R&D for a number of companies including start-ups, focusing mainly on air interface and circuit aspects, as well as being involved in a number of standards and M&A activities. He is retired from u-blox AG, where he worked on new standards for IoT communications and key cellular RF implementation technologies. He is a Life Member of the IEEE, and serves on the boards of Cambridge Wireless and the IoT Security Foundation.